iScience

CellPress
OPEN ACCESS

Article

Dental pulp stem cells accelerate wound healing through CCL2-induced M2 macrophages polarization

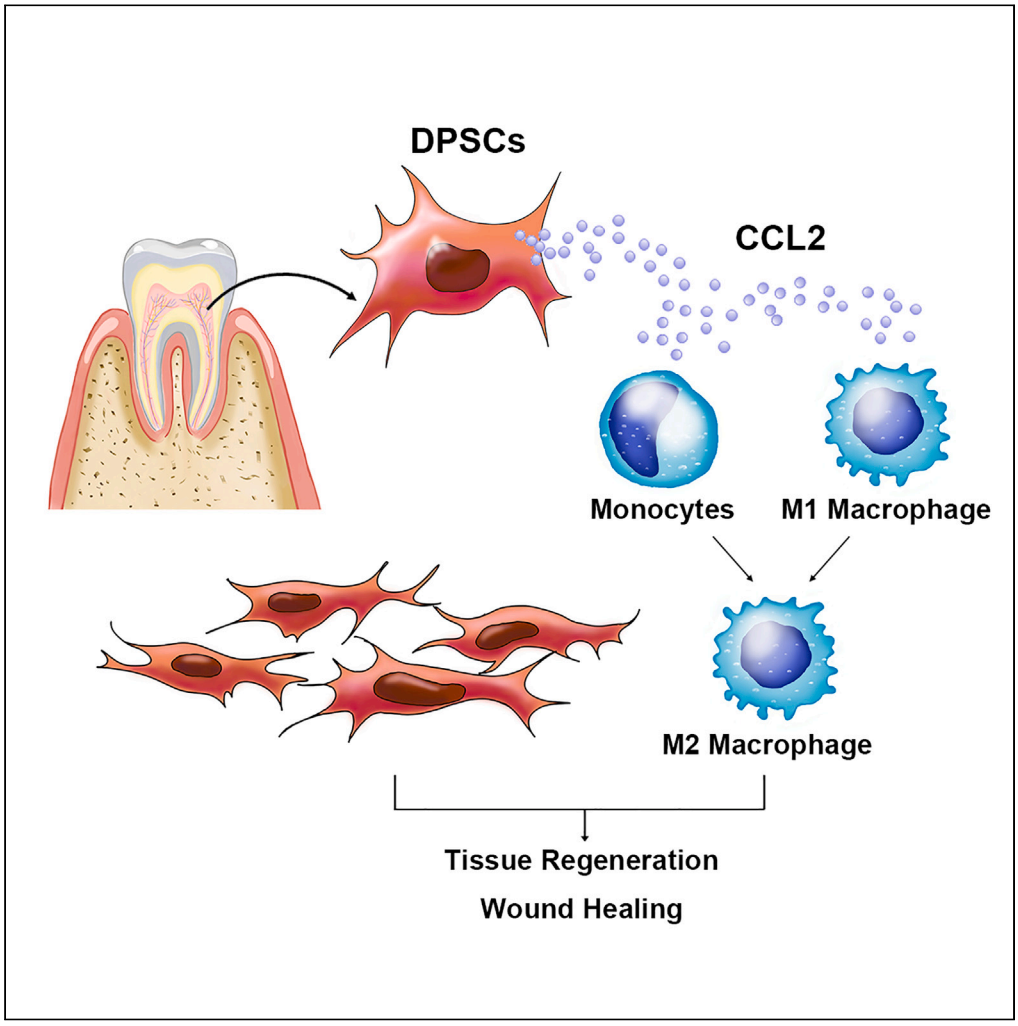

Zi Yang, Linsha Ma, Conglin Du, Jingsong Wang, Chunmei Zhang, Lei Hu, Songlin Wang

hulei@ccmu.edu.cn (L.H.)
slwang@ccmu.edu.cn (S.W.)

Highlights

DPSCs exhibited enhanced tissue regeneration and wound healing potential

DPSCs exhibited higher expression levels of CCL2

DPSCs promote the polarization of M2 macrophages via secreting CCL2

DPSCs promoted wound healing through CCL2-induced M2 macrophages polarization

Yang et al., iScience *26*, 108043
October 20, 2023
https://doi.org/10.1016/j.isci.2023.108043

iScience

CellPress
OPEN ACCESS

Article

Dental pulp stem cells accelerate wound healing through CCL2-induced M2 macrophages polarization

Zi Yang,[1] Linsha Ma,[1,2] Conglin Du,[1,2] Jingsong Wang,[1,2,3] Chunmei Zhang,[1,2] Lei Hu,[1,2,4,7,*] and Songlin Wang[1,2,3,5,6,*]

SUMMARY

The crosstalk between mesenchymal stem cells (MSCs) and the host immune function plays a key role in the efficiency of tissue regeneration and wound healing. However, the difference in immunological modulation and tissue regeneration function between MSCs from different sources remains unclear. Compared to PDLSCs, BMMSCs, and ADSCs, DPSCs exhibited greater tissue regeneration potential and triggered more M2 macrophages *in vivo*. DPSCs elicited the polarization of M2a macrophages by conditioned medium and transwell assay and exhibited higher expression levels of C-C motif chemokine ligand 2 (CCL2). Specific blocking of CCL2 could significantly inhibit the DPSCs-induced polarization of M2 macrophages. DPSCs promoted wound healing of the palatal mucosa and M2 macrophages polarization *in vivo*, which could be significantly impaired by CCL2-neutralized antibody. Our data indicate that DPSCs exert better tissue regeneration potential and immunoregulatory function by secreting CCL2, which can enhance MSCs-mediated tissue regeneration or wound healing.

INTRODUCTION

Mesenchymal stem cells (MSCs) are self-renewable and multipotent stromal cells which can differentiate into various cell types, such as osteoblasts, chondrocytes, myocytes, and adipocytes.[1,2] In addition to their multiple differentiation potential, MSCs are capable of regulating various immune cells associated with both innate and adaptive immune systems.[2,3] The differentiation and immunoregulatory capacity of MSCs make them suitable for wide clinical applications in various tissue regeneration, defect repair, and immunological diseases.[2–5] Evidence has shown that the tissue regeneration function is largely impaired when MSCs are transplanted in wild-type mice compared to immune-deficient nude mice.[6] This indicated an intricate interaction between MSCs and the host immune function. To date, various functions and mechanisms have been identified between MSCs and host immune function.

On the one hand, MSCs regulate the phenotype and function of immune cells that participate in tissue repair and regeneration through a synergy of cell contact-dependent mechanisms and soluble factors.[3–5] MSCs express Fas ligand (FasL) to induce T cell apoptosis through the FasL/Fas pathway[7,8] and suppress B cell proliferation through programmed cell death protein 1 and programmed cell death 1 ligand interaction in a cell-to-cell contact-dependent manner.[9] Meanwhile, the secretomes of MSCs, including transforming growth factor β1 (TGF-β1),[10] indolamine 2,3-dioxygenase (IDO),[11] and prostaglandin E2,[12] play pivotal roles in immunomodulation and tissue repair.[3–5] On the other hand, pro-inflammatory T cells in the recipients inhibited bone marrow mesenchymal stem cells (BMMSCs)-mediated bone formation via T helper 1 cytokine interferon (IFN)-γ and tumor necrosis factor (TNF)-α.[6] These results indicate that crosstalk between implanted donor MSCs and recipient immune cells may govern MSCs-mediated tissue regeneration; however, the different sources of MSCs-mediated immunomodulation during tissue regeneration need to be investigated.

In the present study, we chose human mesenchymal stem cells including BMMSCs, periodontal ligament stem cells (PDLSCs), adipose-derived stem cells (ADSCs), and dental pulp stem cells (DPSCs), which are widely used in clinical applications. The MSCs were induced to form cell sheets by vitamin C[13,14] and transplanted subcutaneously into C57BL/6 mice carried by hydroxyapatite/tricalcium phosphate (HA/TCP). Eight weeks after transplantation, the tissue regeneration potential and immune response were analyzed, and the underlying

[1]Salivary Gland Disease Center and Beijing Key Laboratory of Tooth Regeneration and Function Reconstruction, Beijing Laboratory of Oral Health and Beijing Stomatological Hospital, Capital Medical University, Beijing, China
[2]Immunology Research Center for Oral and Systemic Health, Beijing Friendship Hospital, Capital Medical University, Beijing, China
[3]Department of Biochemistry and Molecular Biology, Capital Medical University School of Basic Medicine, Beijing, China
[4]Department of Prosthodontics, Beijing Stomatological Hospital, Capital Medical University, Beijing, China
[5]Laboratory for Oral and General Health Integration and Translation, Beijing Tiantan Hospital, Capital Medical University, Beijing, China
[6]Research Units of Tooth Development and Regeneration, Chinese Academy of Medical Sciences, Beijing, China
[7]Lead contact
*Correspondence: hulei@ccmu.edu.cn (L.H.), slwang@ccmu.edu.cn (S.W.)
https://doi.org/10.1016/j.isci.2023.108043

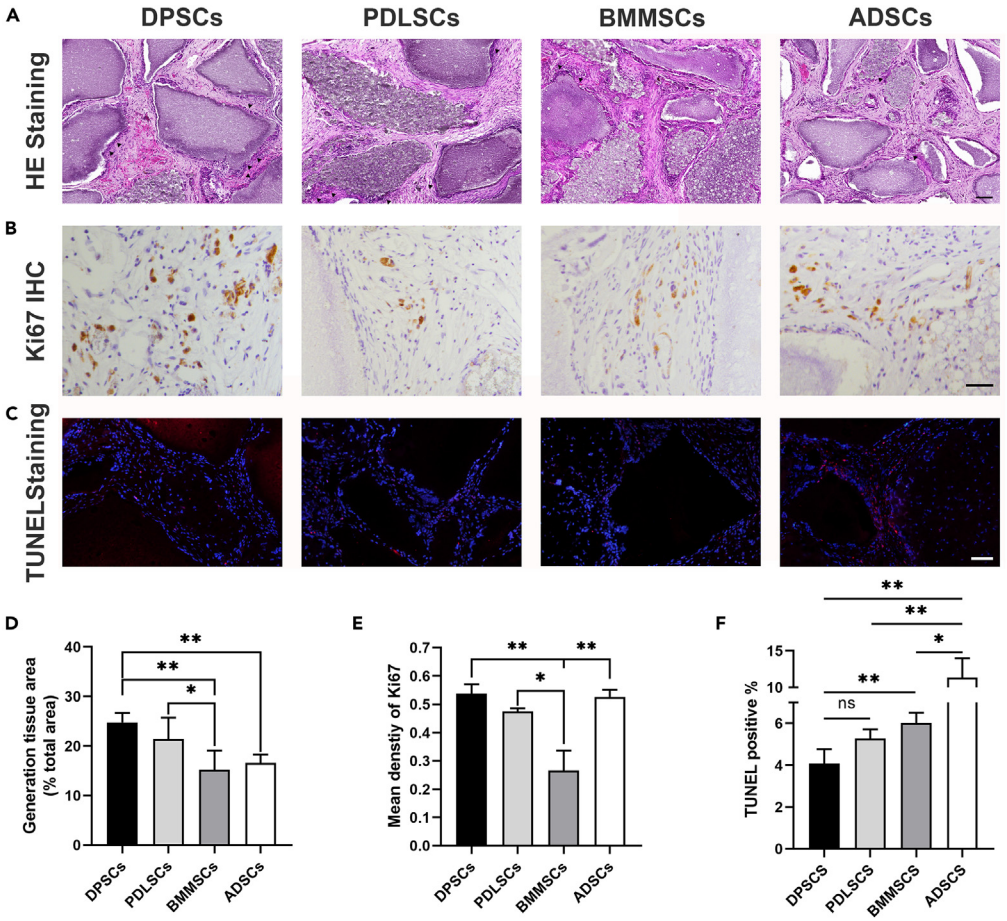

Figure 1. DPSCs sheet exhibited higher tissue regeneration potential in C57BL6 mice compared to BMMSCs and ADSCs

(A and D) HE staining and quantitative analysis results revealed a more mineralized collagen-like matrix (black arrow) was regenerated in the DPSCs group compared to the BMMSCs and ADSCs groups (scale bar: 200 μm).

(B and E) Immunohistochemical staining and quantitative analysis showed that Ki67 was highly expressed in the DPSCs and ADSCs groups compared to the BMMSCs groups (scale bar: 50 μm).

(C and F) TUNEL staining indicated that the DPSCs group showed a lower positive percentage compared with the BMMSCs and ADSCs groups (scale bar: 100 μm) ($^{ns}P > 0.05$, *p < 0.05, **p < 0.01).

molecular mechanisms of MSCs were investigated. The present study sheds light on the function and mechanism of intricate interactions between MSCs and the host immune system and provides strategies for enhancing the efficacy and ability of MSCs in tissue regeneration.

RESULTS

DPSCs sheet exhibited higher tissue regeneration potential than BMMSCs and ADSCs sheets in C57BL6 mice

Human DPSCs, PDLSCs, BMMSCs, and ADSCs sheets with carrier HA/TCP particles were subcutaneously implanted into C57BL6 mice. Eight weeks after transplantation, the animals were sacrificed, and the grafts were harvested for histological analysis. HE staining and quantitative analysis results revealed that a more mineralized collagen-like matrix was regenerated in the DPSCs and PDLSCs group compared to the BMMSCs and ADSCs groups ($p < 0.05$ or $p < 0.01$) (Figures 1A and 1D). Furthermore, immunohistochemical staining and quantitative analysis showed that Ki67 was highly expressed in the DPSCs, PDLSCs, and ADSCs groups compared to the BMMSCs groups ($p < 0.05$, $p < 0.01$) (Figures 1B and 1E). Moreover, TUNEL staining indicated that the DPSCs group showed a lower positive percentage compared with BMMSCs and ADSCs groups ($p < 0.01$) (Figures 1C and 1F).

DPSCs induce polarization of macrophages toward CD206$^+$ M2 phenotype during tissue regeneration

We next investigated the *in vivo* effects of human DPSCs, PDLSCs, BMMSCs, and ADSCs on the inflammatory cell response. Based on immunohistochemical staining, the ratio of CD68$^+$ to CD206$^+$ cells (M2 macrophages) was significantly increased in DPSCs and ADSCs treatment as compared to the PDLSCs and BMMSCs groups ($p < 0.01$) (Figures 2A and 2B). qRT-PCR analysis showed that the expression of *Cd68* did not

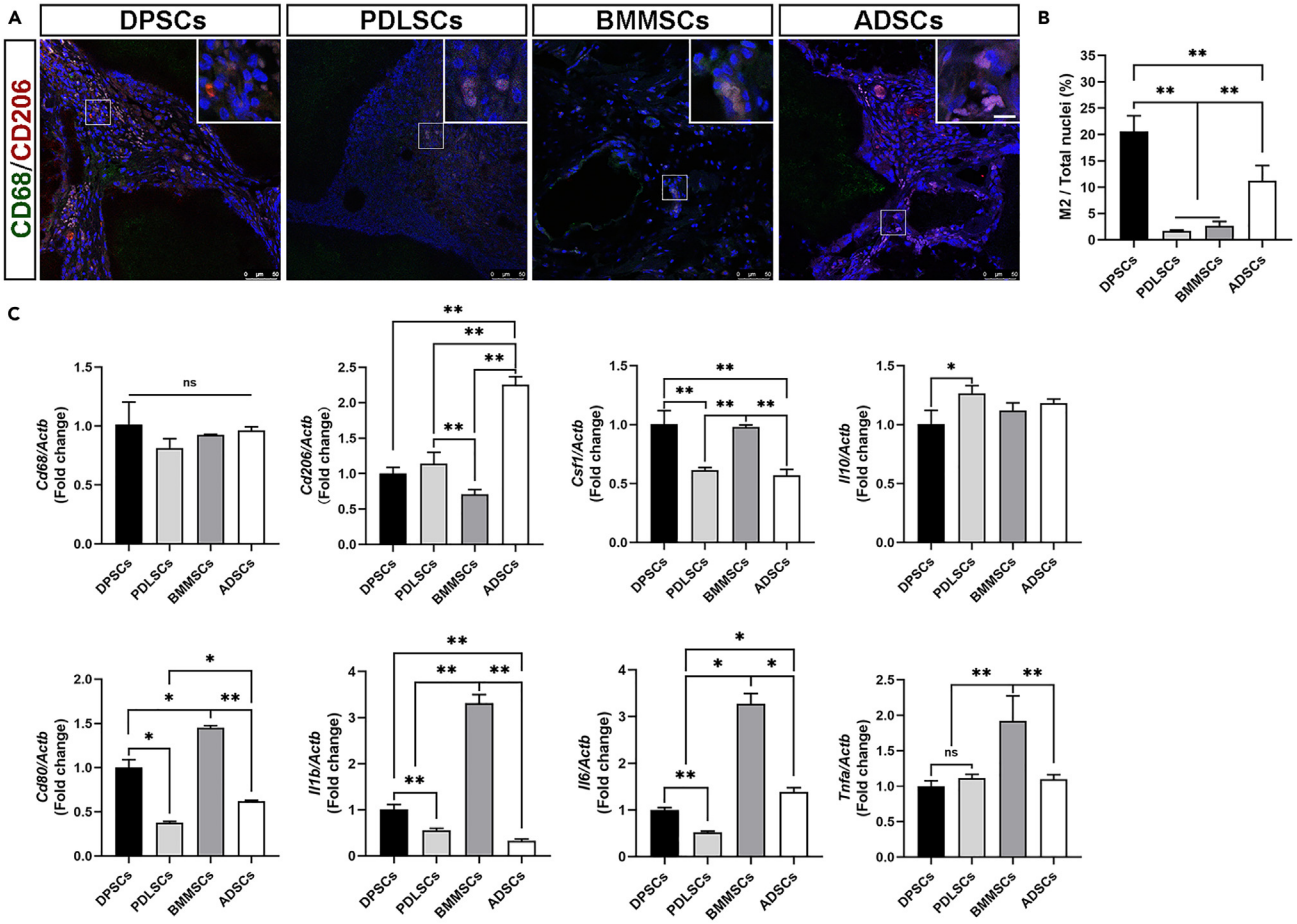

Figure 2. DPSCs induces polarization of macrophages toward CD206+ M2 phenotype during tissue regeneration

(A) Translation sections were dual-color immunostained with specific antibodies for CD68 (Green) and CD206 (Red) (Scale bar: 50 and 10 μm).

(B) The number of $CD68^{+}$ to CD206+ cells (M2 macrophages) was significantly increased in DPSCs and ADSCs treatment as compared to the PDLSCs and BMMSCs groups.

(C) Real-time PCR analysis revealed that the DPSCs could induce more M2 macrophage-related genes *in vivo* compared with BMMSCs ($^{ns}P > 0.05$, *p < 0.05, **p < 0.01).

differ between the different groups, but DPSCs reduced the expression of *Cd80*, *Tnfa*, *Il1b*, and *Il6*, compared with the BMMSCs group, and induced the expression of *Csf1* compared with ADSCs and PDLSCs ($p < 0.05$, $p < 0.01$) (Figure 2C).

DPSCs-CM converted human THP-1 monocytes to M2 macrophages

THP-1 to M0 macrophages were activated by pulsing with phorbol 12-myristate 13-acetate (100 ng/mL). M0 macrophages were cultured with DPSCs-conditioned medium (CM) and BMMSCs-CM for 1 and 3 days. Double immunofluorescence staining of CD68 and CD80 showed that DPSCs-CM and BMMSCs-CM could both significantly inhibit the polarization of M1 macrophages for 3 days ($p < 0.01$) (Figures 3A and 3C). Immunocytochemical staining of CD68 and CD163 showed that DPSCs-CM and BMMSCs-CM could both significantly elicit polarization of M2 macrophages for 3 days, but the ability of BMMSCs-CM was weaker than that of DPSCs ($p < 0.01$) (Figures 3B and 3E). Cultured by DPSCs-CM and BMMSCs-CM for 3 days, the secretion of TNF-α of THP-1 macrophages was decreased and IL-10 was increased, and there was no significant difference between DPSCs-CM and BMMSCs-CM treatments ($p < 0.05$, $p < 0.01$) (Figures 3D and 3F). For the expression of mRNA of pro-inflammatory and anti-inflammatory cytokines, qRT-PCR analysis showed that *IL6*, *TNFA*, *IL10*, and *ARG1* mRNA expression for 1 day was upregulated, whereas *IL6* and *TNFA* mRNA expression levels were downregulated and *IL10* and *ARG1* mRNA expression levels were upregulated for 3 days. The immunomodulating function of DPSCs-CM was significantly better than that of BMMSCs-CM for 3 days ($p < 0.05$, $p < 0.01$) (Figure 3G). For the M2 macrophage subtype, we chose *YM1*, *ARG1*, *IL1RA*, *PPARG*, *JMJD3*, and *SOCS1* as M2a marker, *SPHK1* and *LIGHT* as M2b marker, and *TGFB1*, *MERTK*, and *RETNLB* as M2c marker. And DPSCs-CM could elicit the polarization of M2a, but not M2b and M2c (Figure 3H).

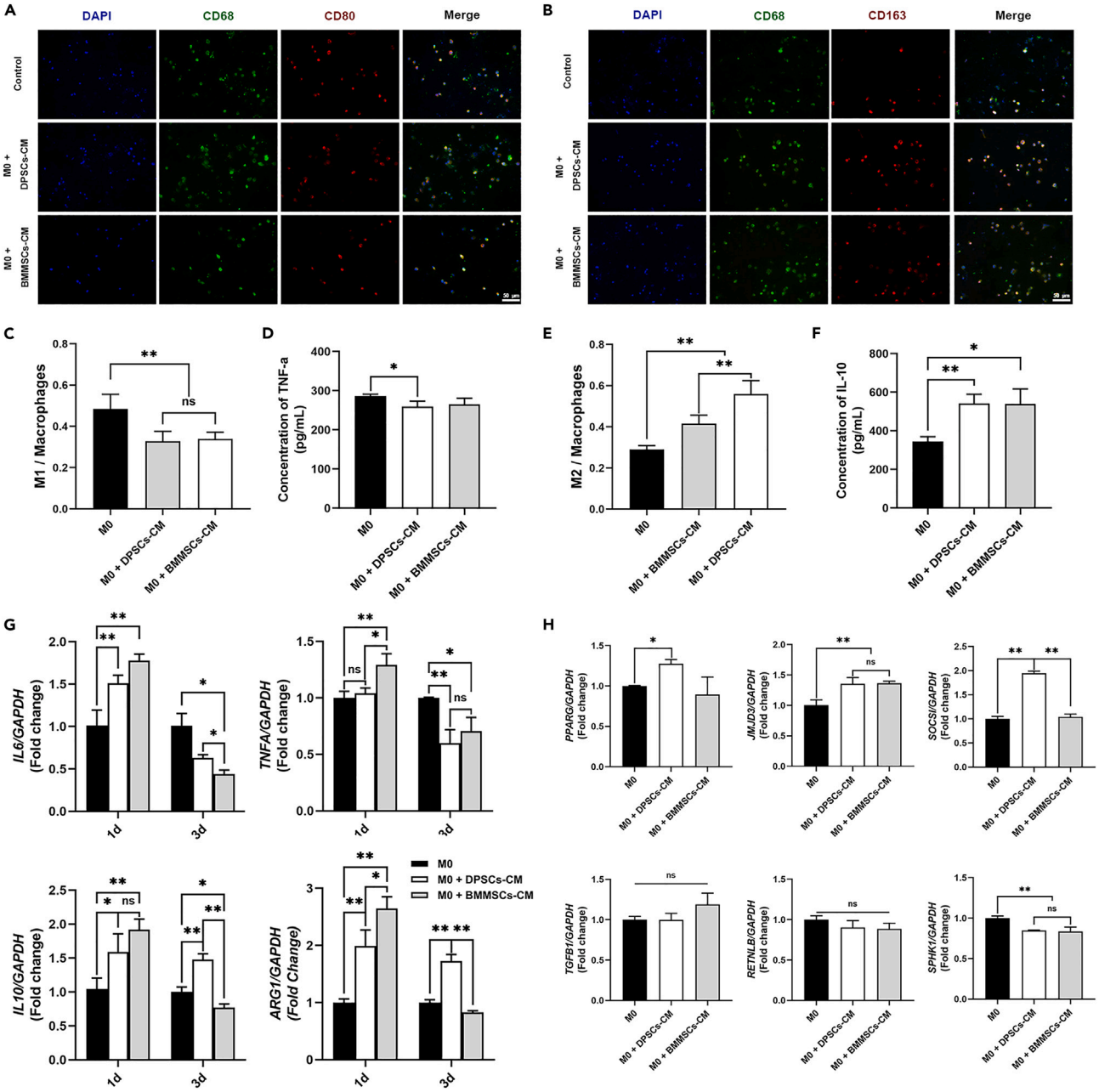

Figure 3. DPSCs-CM converted human THP-1 monocytes to M2 macrophages

(A and C) Double immunofluorescence staining of CD68 and CD80 revealed that DPSCs-CM and BMMSCs-CM could both significantly inhibit the polarization of M1 macrophages for 3 days (Scale bar: 50 μm).

(B and E) Immunocytochemical staining of CD68 and CD163 showed that DPSCs-CM and BMMSCs-CM could both significantly elicit polarization of M2 macrophages for 3 days, but the ability of BMMSCs-CM was weaker than that of DPSCs (Scale bar: 50 μm).

(D and F) After the co-culture, the secretion of TNF-α of THP-1 macrophages was decreased and IL-10 was increased, and there was no significant difference between DPSCs-CM and BMMSCs-CM treatments.

(G) qRT-PCR analysis showed that *IL6*, *TNFA*, *IL10*, and *ARG1* mRNA expression for 1 day was upregulated, whereas *IL6* and *TNFA* mRNA expression levels were downregulated and *IL10* and *ARG1* mRNA expression levels were upregulated for 3 days after treated with DPSCs-CM. The immunomodulating ability of DPSCs-CM was significantly better than that of BMMSCs-CM.

(H) qRT-PCR analysis showed that after treated with DPSCs-CM, M2a macrophages-related mRNA expression of *PPARG*, *SOCS1*, and *JMJD3* was upregulated, whereas *SPHK1* mRNA expression levels were downregulated for 3 days. The mRNA expression of *TGFB1* and *RETNLB* did not differ from the control group. Data are presented as mean ± SD of three independent experiments ($^{ns}P > 0.05$, *p < 0.05, **p < 0.01).

DPSCs elicit the polarization of M2 macrophages in transwell assay

The M0 macrophages were co-cultured with DPSCs and BMMSCs at passage 3–5 at a ratio of 2:1 (macrophages: stem cells) cell density by transwell test for 3 days. Similar to MSCs-CM, DPSCs and BMMSCs could significantly inhibit the polarization of M1 macrophages and elicit polarization of M2 macrophages for 3 days by transwell with respect to immunofluorescence staining; the ability of BMMSCs was significantly weaker than that of DPSCs ($p < 0.01$) (Figures 4A–4C and 4E). The secretion of TNF-α in THP-1 macrophages was significantly decreased, and IL-10 was significantly increased after co-cultured with DPSCs (Figures 4D and 4F). qRT-PCR analysis showed that *IL1B* and *TNFA* mRNA expression was downregulated for 1 day, whereas *IL1B*, *IL6*, and *TNFA* mRNA expression levels were downregulated after co-cultured with DPSCs for 3 days. The mRNA expression of *ARG1* was upregulated for 1 and 3 days, but the ability of BMMSCs was significantly weaker than that of DPSCs ($p < 0.05$, $p < 0.01$) (Figure 4G). For M2 macrophages subtype, we found that DPSCs could induce the polarization of M2a and M2c, but not M2b by transwell assay (Figure 4H). This evidence showed that DPSCs and BMMSCs could elicit the polarization of M2 macrophages from M0 macrophages via soluble cytokines, and that DPSCs possess better immunomodulatory function than BMMSCs.

DPSCs could convert human THP-1 M1 macrophages to M2 macrophages

For M1 polarization, M0 in fresh medium were co-stimulated with lipopolysaccharide (1 μg/mL) and IFNγ (50 ng/mL), and M0 were incubated with the corresponding stimuli for 24 h without media replacement. qRT-PCR analysis showed that M2a-related genes, such as *PPARG* and *YM1*, were significantly upregulated in DPSCs-CM and BMMSCs-CM group, but the ability of BMMSCs was significantly weaker than that of DPSCs ($p < 0.05$, $p < 0.01$). Meanwhile, in the DPSCs-CM and BMMSCs-CM group, the M2b- and M2c-related genes did not differ from control group (Figure S1A). This evidence demonstrated that DPSCs and BMMSCs could elicit the polarization of M2a macrophages from M1 macrophages. In transwell assay, qRT-PCR analysis showed that M1- and M2b-related genes, for instance *IL1B*, *TNFA*, and *IL6*, were downregulated after co-cultured with DPSCs and BMMSCs for 3 days. DPSCs and BMMSCs could stimulate the M2a and M2c polarization, but not M2b (Figure S1B).

DPSCs-mediated induction of M2 macrophages by CCL2

Gene expression datasets were used to compare gene expression between human BMMSCs and DPSCs. The top 20 differentially expressed genes related to immunity between DPSCs and BMMSCs were visualized (Figure 5A). These results were confirmed by qRT-PCR analysis, demonstrating that the mRNA expression levels of *CCL2*, *TGFBR3*, *C1S*, *IL1R1*, *IL10RB*, *IFNAR1*, *CD46*, and *CD302* were decreased in BMMSCs at passage three compared to those of DPSCs (Figure 5B). The concentration of CCL2 secreted by DPSCs was significantly higher than that secreted by BMMSCs ($p < 0.001$, Figure 5C).

To confirm the function of CCL2 in this immunomodulatory process, macrophages were co-cultured with DPSCs and BMMSCs at passage 4 in transwell for 3 days in the presence or absence of specific neutralizing antibodies for CCL2 (10 μg/mL) and CCL2 recombinant protein (15 ng/mL). With respect to mRNA expression, DPSCs and BMMSCs could downregulate the mRNA expression of *IL1B*, *IL6*, and *TNFA*, and upregulate the mRNA expression of *ARG1*, and blocking CCL2 could inhibit the DPSCs-mediated decrease of pro-inflammatory cytokines ($p < 0.05$ or $p < 0.01$). However, the presence of neutralizing antibodies against CCL2 did not influence the immunomodulatory function of BMMSCs (Figures 6A–6D). Meanwhile, DPSCs and BMMSCs could upregulate the concentration of IL-10 secreted and downregulate the concentration of TNF-α secreted and blocking CCL2 could inhibit DPSCs-mediated induction of M2 macrophages, but not BMMSCs ($p < 0.05$ or $p < 0.01$) (Figures 6E and 6F).

Passage-induced senescence of DPSCs still possesses the ability to induce M2 macrophages polarization via CCL2

MSCs cultured at passage 6 had a senescence phenotype, and we chose DPSCs at passage eight to examine their immunomodulatory function on macrophages of senescent DPSCs. DPSCs (P8) downregulated the mRNA expression of IL1B, IL6, and TNFA and upregulated the expression of IL10 for 3 days. Blocking CCL2 could inhibit DPSCs (P8)-mediated induction of M2 macrophages (Figures 7A–7F). ARG1 protein expression was upregulated by culturing with DPSCs (P8) in transwell for 3 days, and specific neutralizing antibodies of CCL2 could weaken this ability of DPSCs ($p < 0.05$ or $p < 0.01$) (Figures 7G and 7H). This evidence proved that CCL2 secreted by DPSCs plays an important role in the induction of M2 macrophages.

DPSCs-based therapy enhanced mucosa wound healing in mice via CCL2

Given the important roles of both MSCs and M2 macrophages in wound healing, we investigated the function of MSCs and CCL2 in wound healing models of palates in mice. First, we explored whether DPSCs and BMMSCs were capable of enhancing mucosal excisional wound repair. DPSCs and BMMSCs (2.5×10^5 per mouse) and recombinant human CCL2 (10 μg per mouse) were directly injected into the surrounding mucosa on day 1, and neutralizing antibodies of human CCL2 were administered to mice by intraperitoneal injection on day 2 at a dose of 10 μg/mouse. Wound closure was carefully measured on day 5. Our results showed that mice receiving DPSCs infusion displayed accelerated mucosal wound closure compared with the control mice without treatment, and the application of CCL2 neutralizing antibodies inhibited DPSCs-mediated wound repair, but not BMMSCs ($p < 0.01$) (Figures 8A and 8B). The usage of human CCL2 recombinant protein and neutralizing antibodies did not differ from the control group ($p > 0.05$; Figure S2A, B). Histological analysis of wounds on day 5 showed a more organized granulation tissue at the excisional wound site in DPSCs-treated mice compared with other groups (Figures 8C and S2C).

Next, we investigated the *in vivo* effects of DPSCs and BMMSCs on the phenotype of macrophages in mucosal wounds. Dual-color immunofluorescence assays were performed using specific antibodies CD68 and ARG1, which are well-known markers of M2 macrophages. DPSCs

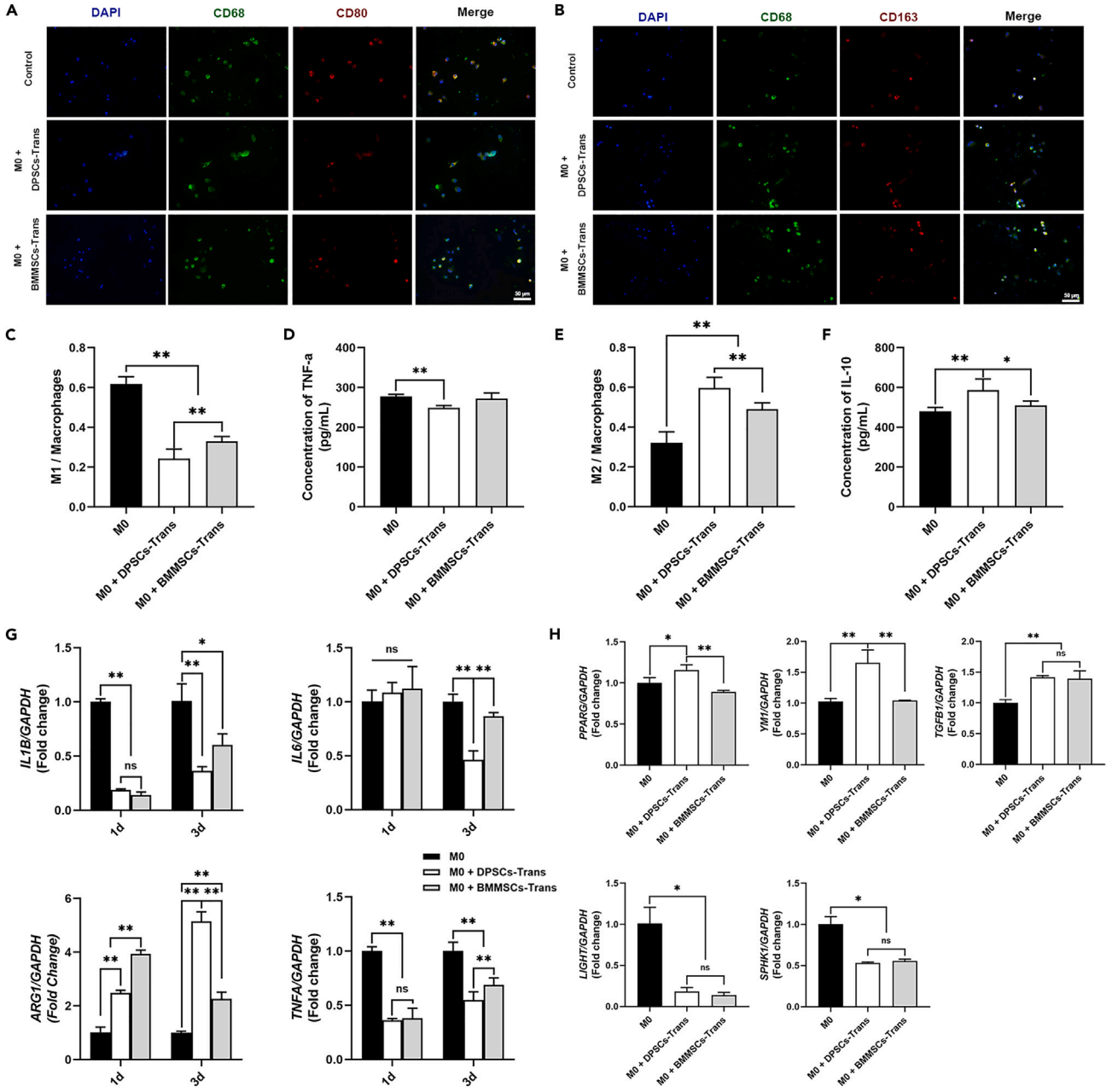

Figure 4. DPSCs elicit the polarization of M2 macrophages in transwell assay

(A and C) Immunocytochemistry staining of CD68 and CD80 showed that DPSCs and BMMSCs could both significantly inhibit the polarization of M1 macrophages for 3 days by transwell, and the ability of BMMSCs was significantly weaker than that of DPSCs (Scale bar: 50 μm).

(B and E) Immunocytochemistry staining of CD68 and CD163 showed that DPSCs and BMMSCs could both significantly elicit polarization of M2 macrophages for 3 days by transwell, but the ability of BMMSCs was weaker than DPSCs (Scale bar: 50 μm).

(D and F) THP-1 cell lines cultured with DPSCs could increase the concentration of IL-10 and decrease the concentration of TNF-α for 3 days, and the ability of BMMSCs was significantly weaker than DPSCs.

(G) qRT-PCR analysis showed that *IL1B* and *TNFA* mRNA expression for 1 day was downregulated, whereas *IL1B*, *IL6*, and *TNFA* mRNA expression levels were downregulated for 3 days. The mRNA expression of *ARG1* was upregulated for 1 and 3 days, but the ability of BMMSCs was significantly weaker than that of DPSCs.

(H) qRT-PCR analysis showed that *PPARG* and *YM1* mRNA expression was upregulated, and mRNA expression of *SPHK1* and *LIGHT* in DPSCs-Trans group was downregulated for 3 days. M2c macrophage marker *TGFB1* mRNA expression was upregulated in DPSCs-trans and BMMSCs-trans group. Data are presented as mean ± SD of three independent experiments ($^{ns}P > 0.05$, *p < 0.05, **p < 0.01).

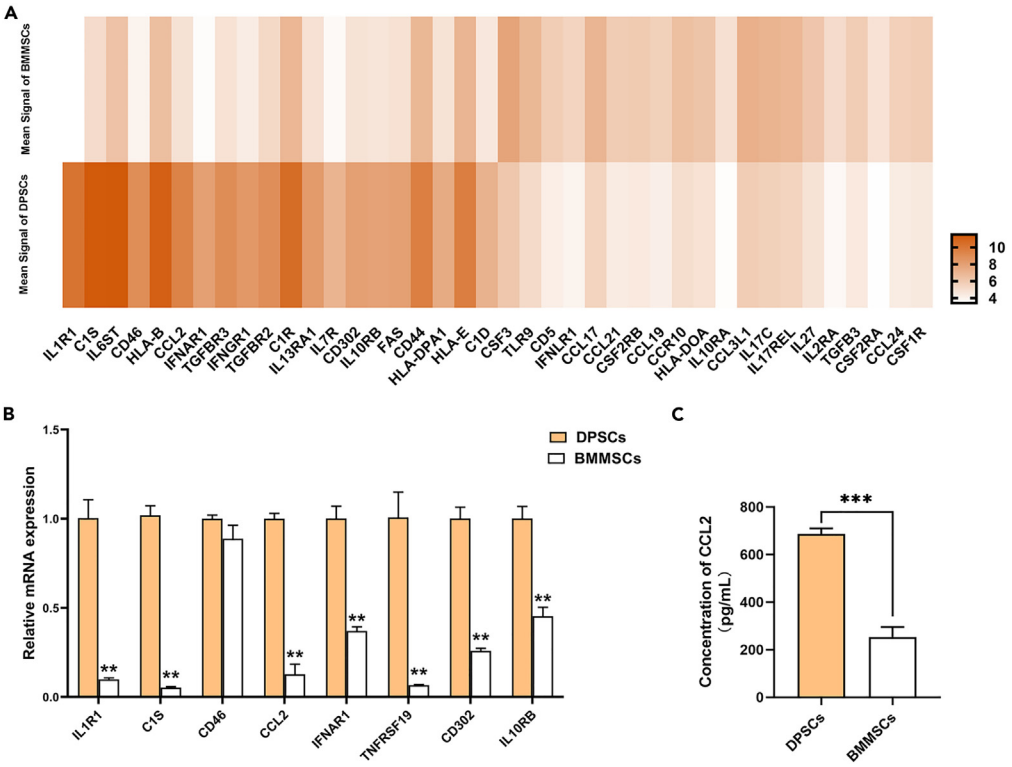

Figure 5. Bioinformatic analysis gene expression profile of BMMSCs and DPSCs

(A) Top 20 differentially expressed genes related to immunity between DPSCs and BMMSCs were visualized.

(B) qRT-PCR analysis demonstrated that the mRNA expression levels of *CCL2*, *TGFBR3*, *C1S*, *IL1R1*, *IL10RB*, *IFNAR1*, *CD46*, and *CD302* were decreased in BMMSCs at passage three compared to those of DPSCs.

(C) ELISA analysis showed that the concentration of CCL2 secreted by DPSCs was significantly higher than that of BMMSCs. Values are means ± SDs. Student's t-tests were used to determine statistical significance. (**$p < 0.01$; ***$p < 0.001$).

and BMMSCs treatment led to an increase in the number of CD68- and ARG1-positive macrophages compared with the control group, and the percentage of M2 macrophages was significantly higher in the DPSCs group than in the BMMSCs group ($p < 0.05$) (Figures 8D and 8E). Meanwhile, the application of neutralizing antibody weakened this function of DPSCs, but not BMMSCs ($p < 0.01$) (Figures 8D and 8E). The usage of CCL2 recombinant protein and neutralizing antibodies did not differ from the control group ($p > 0.05$; Figures S2D and S2E). These findings suggest that DPSCs are capable of promoting the polarization of M2 macrophages and enhancing the healing of excisional mucosa in mice, and that CCL2 plays an essential role in the immunomodulatory activity of DPSCs.

DISCUSSION

MSCs-based regenerative medicine is a promising strategy for tissue regeneration and wound healing.[3] MSCs display great properties of mineral tissue regeneration in nude mice.[6,15] However, until now, the application of MSCs influenced by the crosstalk between MSCs and the immune system of recipients was still unstable and limited in clinical trials. MSCs from different sources possess different characteristics associated with immunomodulation.[16] Dental-tissue-derived MSCs, such as DPSCs, PDLSCs, and SCAPs, residing in human teeth and dental tissue, have been isolated and characterized, and exhibit different characteristics.[1,17] Due to their neural crest origin, dental-derived MSCs have stronger stemness and neurogenic capacity.[18] Our previous study demonstrated that BMMSCs, ADSCs, DPSCs, and PDLSCs possess different capacities for tissue regeneration and varying immunomodulatory priority, providing evidence for selecting suitable MSCs based on different characteristics in clinical application. With greater proliferation and colony-forming properties and higher expression levels of the *ALP*, *DSPP*, *and DMP1*,[19] DPSCs have a superior ability to maintain their stem cell properties during aging and have greater resistance under conditions of inflammation-induced senescence.[20] In the present study, at the passage eight, the proliferation level of BMMSCs is significantly lower than that of DPSCs, and DPSCs still possess immunomodulation ability to macrophages. The high resistance to cellular senescence of DPSCs plays an important role in the potential of MSCs for disease therapy.

Local administration of allogeneic or autogenous BMMSCs, PDLSCs, and DPSCs could induce tissue regeneration in periodontal defects *in vivo*, and more hard tissue regeneration in the periodontium after DPSCs injection compared to BMMSCs injection *in vivo*.[9,12,20–24] Vitamin C could induce complete cell sheet formation of MSCs, and enhanced bone regeneration, osteoblastic differentiation, and extracellular matrix production.[13,14] Thus, in the present study, we transplanted four different cell sheet and found DPSCs showed greater potential to

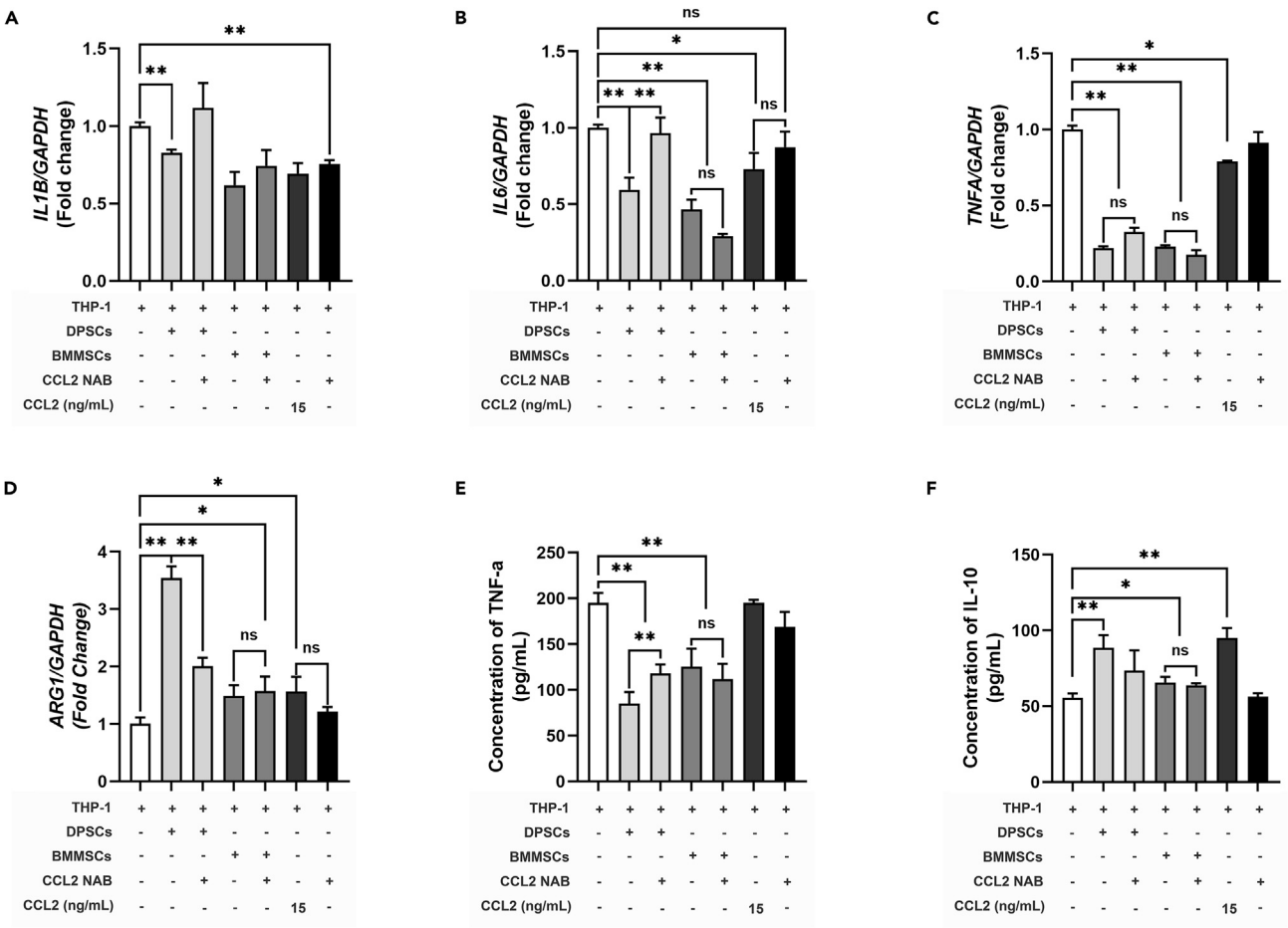

Figure 6. DPSCs-mediated induction of M2 macrophages by CCL2

(A–D) DPSCs could downregulate the mRNA expression of *IL1B*, *IL6*, and *TNFA*, and upregulate the mRNA expression of *ARG1*, and blocking CCL2 could inhibit the DPSCs-mediated decrease of pro-inflammatory cytokines. The presence of neutralizing antibodies against CCL2 did not influence the immunomodulatory function of BMMSCs.

(E and F) DPSCs could increase the concentration of IL-10 and decrease the concentration of TNF-α for 3 days, and blocking CCL2 could inhibit DPSCs-mediated induction of M2 macrophages, but not BMMSCs ($^{ns}P > 0.05$, *p < 0.05, **p < 0.01). NAB: neutralizing antibody.

enhance tissue regeneration with higher expression of proteins related to proliferation and less apoptosis compared to BMMSCs and ADSCs. In wound healing models, DPSCs possess great ability to accelerate wound closure compared to BMMSCs.

The interaction between implanted donor MSCs and recipient immune cells may play an essential role in MSC-mediated tissue regeneration.[2–5] Meanwhile, the immunomodulatory functions of MSCs from different sources varied *in vitro* and *in vivo*. BMMSCs, ADSCs, and MSCs of dental tissue can suppress the proliferation of T cells, B cells, natural killer cells, and other immune cells.[16,25] This might partially be explained by the fact that MSCs from different sources and under different culture conditions express different surface markers and show varying cytokine secretion profiles. Macrophages, one of the major types of innate immune cells, play essential roles in inflammation, immunity, tissue regeneration, and tissue repair via classic (M1) and alternative (M2) polarization. M1 macrophages play important roles in inflammation by secreting pro-inflammatory mediators, including IL-1, IL-6, TNF-α, and IL-12. In contrast, M2 macrophages are characterized by the secretion of high levels of anti-inflammatory mediators, such as IL-10 and TGF-β.[26–28]

In the present study, we found that macrophages, which partly govern tissue regeneration, showed different polarization patterns after translation of MSCs from different sources. Some studies have reported communication between MSCs and macrophages.[29–31] MSCs have been reported to increase macrophages phagocytic capacity.[32] MSCs such as BMMSCs,[33] ADSCs,[30] PDLSCs,[34] and dental follicle stem cells[35] can induce macrophages polarization into the M2 phenotype by stimulating ARG1, CD163, and IL-10 and inhibiting TNF-α. Human gingiva-derived mesenchymal stem cells are capable of eliciting M2 polarization of macrophages, which might contribute to a marked acceleration of wound healing.[31] DPSCs can inhibit macrophages and elicit macrophage M2 polarization via the TNF-α/IDO axis.[11,25] These studies showed different mechanisms of MSC interaction with macrophages.

Based on the expressed markers and secretion profiles, M2-type macrophages could be divided into different subtypes, namely M2a, M2b, M2c, and M2d. The M2a macrophages could express high levels of CD206, decoy receptor IL-1 receptor II, and IL-1 receptor antagonist.

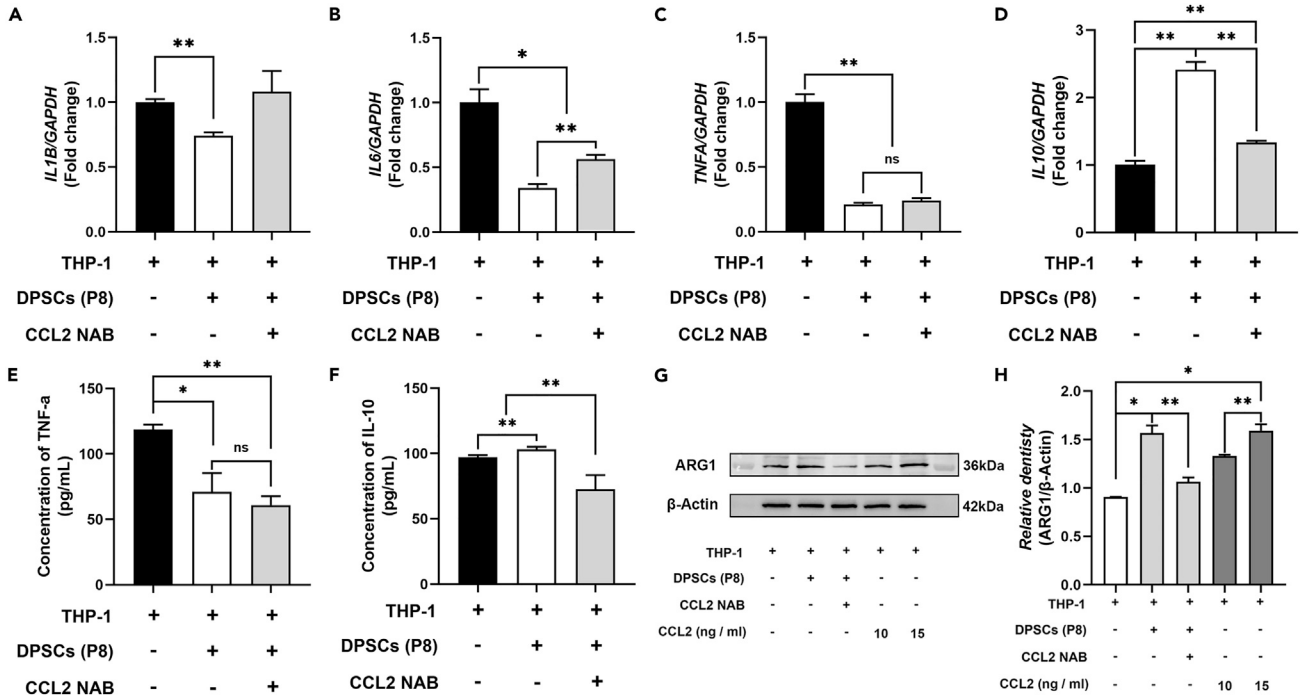

Figure 7. Passage-induced senescence of DPSCs possesses the ability to induce M2 macrophages polarization via CCL2

(A–D) DPSCs (P8) downregulated the mRNA expression of *IL1B*, *IL6*, and *TNFA* and upregulated the expression of *IL10* for 3 days. Blocking CCL2 could inhibit DPSC (P8)-mediated induction of M2 macrophages.

(E and F) DPSCs could increase the concentration of IL-10 and decrease the concentration of TNF-α for 3 days, and blocking CCL2 could inhibit DPSCs (P8)-mediated IL-10 secreting.

(G and H) ARG1 protein expression was upregulated by cultured with DPSCs (P8) in transwell for 3 days, and specific neutralizing antibodies of CCL2 could weaken this ability of DPSCs (P8). ($^{ns}P > 0.05$, *p < 0.05, **p < 0.01). NAB neutralizing antibody.

M2b macrophages produce both anti- and pro-inflammatory cytokines IL-10, IL-1β, IL-6, and TNF-α. M2c subset could release high amounts of IL-10 and TGF-β.[36] In our study, DPSCs and BMMSCs could not only elicit the polarization of M2a by conditioned medium but also induce the M2a and M2c macrophages by transwell assay *in vitro*.

During the process of MSCs-mediated tissue regeneration and repair, MSCs could recruit macrophages via various secreted chemokine, such as CCL2 (monocyte chemotactic protein-1).[37] Through bioinformatic analysis, we found that CCL2 was more highly expressed in DPSCs than in BMMSCs. A previous study reported that CCL2 expressed by a wide array of cell types such as M1 macrophages could modulate monocyte recruitment in multiple inflammatory diseases by interacting with its corresponding receptor, CCR2, which is present in monocytes.[38] The use of neutralizing anti-CCL2 antibody abolished the polarization of THP-1 macrophages mediated by DPSCs, but not BMMSCs, suggesting that CCL2 could contribute to DPSCs-induced polarization of M2 macrophages. CCL2 has been reported to mediate the polarization of macrophages that participate in tissue inflammation. In addition, CCL2 can promote the survival of human CD11b+ peripheral blood mononuclear cells and induce M2 macrophages polarization[39] and decrease TNF-α secretion *in vitro*,[40] but the function is dependent on the MSCs type.[31,41]

Evidence has shown that MSC-derived CCL2 is necessary for the induction of IL-10 expression by macrophages. However, it needs to be combined with other cytokines, as CCL2 alone could not accelerate wound healing in the present study. In the tumor microenvironment, the amplification loop between CCL2 and IL-6 could induce the polarization of M2-type macrophages.[39] Furthermore, CCL2 and C-X-C motif chemokine 12 cooperated as a heterodimer could upregulate the expression of IL-10 of macrophages *in vitro*.[41]

In addition, CCL2 may also play a role in the M1 macrophages. This showed that CCL2 induced bone-marrow-derived macrophages to polarize to the M1 phenotype (pro-inflammatory phenotype) through the CCR2/RhoA axis.[42] Moreover, inhibition of CCL2 by oral administration of bindarit suppressed the infiltration of pro-inflammatory monocytes and altered the inflammatory properties of macrophages in the diabetic periodontium.[43] All these data indicated that CCL2 played an intricate function in the crosstalk between MSCs and macrophages, which needs to be further investigated.

In conclusion, this study demonstrated that DPSCs exert better tissue regeneration potential and immunoregulatory function by secreting CCL2. The results suggest that regulatory effects on macrophages with respect to phenotype and functions during tissue regeneration and wound healing via CCL2 application could enhance MSC-mediated tissue regeneration or wound healing, and an optimized stimulation to enhance DPSCs or other MSC immunomodulation needs to be further investigated.

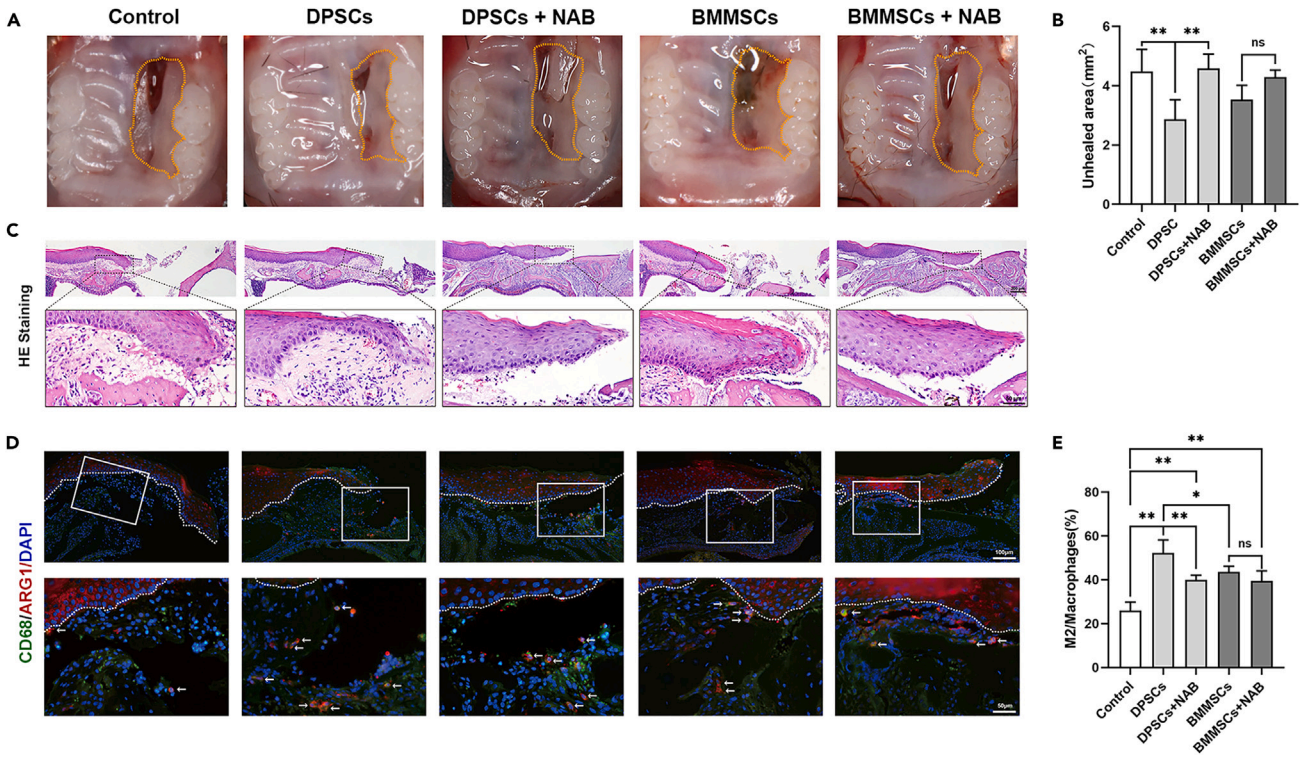

Figure 8. DPSCs-based therapy enhanced mucosa wound healing in mice via CCL2

(A and B) Mice receiving DPSCs infusion displayed accelerated mucosal wound closure compared with the control mice without treatment, and the application of CCL2 neutralizing antibodies inhibited DPSCs-mediated wound repair, but not BMMSCs.

(C) HE staining of wounds showed a more organized granulation tissue at the excisional wound site in DPSCs-treated mice compared with other groups.

(D and E) Double immunofluorescence staining of CD68 and ARG1 revealed DPSCs and BMMSCs treatment led to an increase in the number of M2 macrophages compared with the control group, and the percentage of M2 macrophages was significantly higher in the DPSCs group than in the BMMSCs group, and the application of neutralizing antibody weakened this function of DPSCs, but not BMMSCs ($^{ns}P > 0.05$, *p < 0.05, **p < 0.01). NAB neutralizing antibody.

Limitations of the study

In this study, we demonstrated that compared with other stem cells, DPSCs exert better tissue regeneration potential and immunoregulatory function by secreting CCL2. However, the direct correlation between DPSCs and macrophages in the process of tissue repair was not clear, and the mechanism of how CCL2 further promotes macrophage polarization and tissue regeneration still needs to be explored.

STAR★METHODS

Detailed methods are provided in the online version of this paper and include the following:

- KEY RESOURCES TABLE
- RESOURCE AVAILABILITY
  - Lead contact
  - Materials availability
  - Data and code availability
- EXPERIMENTAL MODEL AND STUDY PARTICIPANT DETAILS
  - Mice
- METHOD DETAILS
  - Mesenchymal cells cultures
  - Transplantation in C57BL/6 mice
  - THP-1 cells culture and stimulation
  - Preparation of conditioned medium (CM)
  - THP-1 cells cultured with CM
  - THP-1 cells co-cultured with BMMSCs and DPSCs by transwell assay
  - Bioinformatic analysis gene expression profile of BMMSCs and DPSCs

- qRT-PCR
- Western blot
- Enzyme-linked immunosorbent assay (ELISA)
- Wound healing model and BMMSCs and DPSCs treatment
- Immunofluorescence staining
- Terminal deoxynucleotidyl transferase dUTP nick end labeling (TUNEL) assay

- QUANTIFICATION AND STATISTICAL ANALYSIS

SUPPLEMENTAL INFORMATION

Supplemental information can be found online at https://doi.org/10.1016/j.isci.2023.108043.

ACKNOWLEDGMENTS

This work was supported by the Beijing Municipal Government grant (Beijing Laboratory of Oral Health, PXM2021-014226-000041), the Beijing Municipal Science and Technology Commission (Z181100001718208), the Beijing Municipal Education Commission (119207020201), the Innovation Research Team Project of Beijing Stomatological Hospital, Capital Medical University (CXTD202201), the Chinese Research Unit of Tooth Development and Regeneration, Academy of Medical Sciences (2019-12M-5-031), the National Natural Science Foundation of China (92049201, 82030031, 81991504, 92149301, L2224038, and 82001067), the Beijing Advanced Innovation Center for Big Data-based Precision Medicine (PXM2021_014226_000026), the Beijing Municipal Government (Beijing Scholar Program, PXM2020_014226_000005 and PXM2021_014226_000020), the Beijing Municipal Colleges and Universities High Level Talents Introduction and Cultivate Project-Beijing Great Wall Scholar Program (CIT&TCD 20180332), and the National Key Research and development Program (2022YFA1104401). Scientific Research Common Program of Beijing Municipal Commission of Education (KM202110025009) and Beijing Municipal Natural Science Foundation (7232071). Young Scientist Program of Beijing Stomatological Hospital, Capital Medical University (YSP202204).

AUTHOR CONTRIBUTIONS

Z.Y. and L.H. contributed to research design; experiment execution; data collection, assembly, and analysis; and manuscript writing. L.M., J.W., and C.Z. contributed to the experiment execution and data analysis and interpretation. C.D. contributed to the data collection, data analysis, and interpretation. S.W. contributed to the study conception and design, financial support, and manuscript writing. All authors read and approved the final manuscript.

DECLARATION OF INTERESTS

The authors declare that they have no competing interests.

INCLUSION AND DIVERSITY

We support inclusive, diverse, and equitable conduct of research.

Received: June 15, 2023
Revised: September 18, 2023
Accepted: September 21, 2023
Published: September 24, 2023

REFERENCES

1. Hu, L., Liu, Y., and Wang, S. (2018). Stem cell-based tooth and periodontal regeneration. Oral Dis. *24*, 696–705. https://doi.org/10.1111/odi.12703.
2. Su, Y., Shi, S., and Liu, Y. (2014). Immunomodulation regulates mesenchymal stem cell-based bone regeneration. Oral Dis. *20*, 633–636. https://doi.org/10.1111/odi.12248.
3. Harrell, C.R., Djonov, V., and Volarevic, V. (2021). The cross-talk between mesenchymal stem cells and immune cells in tissue repair and regeneration. Int. J. Mol. Sci. *22*, 2472. https://doi.org/10.3390/ijms22052472.
4. Weiss, A.R.R., and Dahlke, M.H. (2019). Immunomodulation by mesenchymal stem cells (MSCs): mechanisms of action of living, apoptotic, and dead MSCs. Front. Immunol. *10*, 1191. https://doi.org/10.3389/fimmu.2019.01191.
5. Vasanthan, J., Gurusamy, N., Rajasingh, S., Sigamani, V., Kirankumar, S., Thomas, E.L., and Rajasingh, J. (2020). Role of human mesenchymal stem cells in regenerative therapy. Cells *10*, 54. https://doi.org/10.3390/cells10010054.
6. Liu, Y., Wang, L., Kikuiri, T., Akiyama, K., Chen, C., Xu, X., Yang, R., Chen, W., Wang, S., and Shi, S. (2011). Mesenchymal stem cell-based tissue regeneration is governed by recipient T lymphocytes via IFN-gamma and TNF-alpha. Nat. Med. *17*, 1594–1601. https://doi.org/10.1038/nm.2542.
7. Zhao, Y., Wang, L., Jin, Y., and Shi, S. (2012). Fas ligand regulates the immunomodulatory properties of dental pulp stem cells. J. Dent. Res. *91*, 948–954. https://doi.org/10.1177/0022034512458690.
8. Akiyama, K., Chen, C., Wang, D., Xu, X., Qu, C., Yamaza, T., Cai, T., Chen, W., Sun, L., and Shi, S. (2012). Mesenchymal-stem-cell-induced immunoregulation involves FAS-ligand-/FAS-mediated T cell apoptosis. Cell Stem Cell *10*, 544–555. https://doi.org/10.1016/j.stem.2012.03.007.
9. Liu, O., Xu, J., Ding, G., Liu, D., Fan, Z., Zhang, C., Chen, W., Ding, Y., Tang, Z., and Wang, S. (2013). Periodontal ligament stem cells regulate B lymphocyte function via programmed cell death protein 1. Stem Cell. *31*, 1371–1382. https://doi.org/10.1002/stem.1387.
10. Ding, G., Niu, J., and Liu, Y. (2015). Dental pulp stem cells suppress the proliferation of lymphocytes via transforming growth

factor-beta 1. Hum. Cell *28*, 81–90. https://doi.org/10.1007/s13577-014-0106-y.
11. Lee, S., Zhang, Q.Z., Karabucak, B., and Le, A.D. (2016). DPSCs from inflamed pulp modulate macrophage function via the TNF-α/IDO axis. J. Dent. Res. *95*, 1274–1281. https://doi.org/10.1177/0022034516657 817.
12. Ding, G., Liu, Y., Wang, W., Wei, F., Liu, D., Fan, Z., An, Y., Zhang, C., and Wang, S. (2010). Allogeneic periodontal ligament stem cell therapy for periodontitis in swine. Stem Cell. *28*, 1829–1838. https://doi.org/10.1002/stem.512.
13. Wei, F., Qu, C., Song, T., Ding, G., Fan, Z., Liu, D., Liu, Y., Zhang, C., Shi, S., and Wang, S. (2012). Vitamin C treatment promotes mesenchymal stem cell sheet formation and tissue regeneration by elevating telomerase activity. J. Cell. Physiol. *227*, 3216–3224. https://doi.org/10.1002/jcp.24012.
14. Bhandi, S., Alkahtani, A., Mashyakhy, M., Abumelha, A.S., Albar, N.H.M., Renugalakshmi, A., Alkahtany, M.F., Robaian, A., Almeslet, A.S., Patil, V.R., et al. (2021). Effect of ascorbic acid on differentiation, secretome and stemness of stem cells from human exfoliated deciduous tooth (SHEDs). J. Pers. Med. *11*, 589. https://doi.org/10.3390/jpm11070589.
15. Hu, L., Zhao, B., Gao, Z., Xu, J., Fan, Z., Zhang, C., Wang, J., and Wang, S. (2020). Regeneration characteristics of different dental derived stem cell sheets. J. Oral Rehabil. *47*, 66–72. https://doi.org/10.1111/joor.12839.
16. Jiang, W., and Xu, J. (2020). Immune modulation by mesenchymal stem cells. Cell Prolif. *53*, e12712. https://doi.org/10.1111/cpr.12712.
17. Hu, L., Zhao, B., and Wang, S. (2018). Stem-cell therapy advances in China. Hum. Gene Ther. *29*, 188–196. https://doi.org/10.1089/hum.2017.224.
18. Huang, G.T.J., Gronthos, S., and Shi, S. (2009). Mesenchymal stem cells derived from dental tissues vs. those from other sources: Their biology and role in regenerative medicine. J. Dent. Res. *88*, 792–806. https://doi.org/10.1177/0022034509340867.
19. Yamada, Y., Fujimoto, A., Ito, A., Yoshimi, R., and Ueda, M. (2006). Cluster analysis and gene expression profiles: a cDNA microarray system-based comparison between human dental pulp stem cells (hDPSCs) and human mesenchymal stem cells (hMSCs) for tissue engineering cell therapy. Biomaterials *27*, 3766–3781. https://doi.org/10.1016/j.biomaterials.2006.02.009.
20. Ma, L., Hu, J., Cao, Y., Xie, Y., Wang, H., Fan, Z., Zhang, C., Wang, J., Wu, C.T., and Wang, S. (2019). Maintained properties of aged dental pulp stem cells for superior periodontal tissue regeneration. Aging Dis. *10*, 793–806. https://doi.org/10.14336/AD.2018.0729.
21. Liu, Y., Zheng, Y., Ding, G., Fang, D., Zhang, C., Bartold, P.M., Gronthos, S., Shi, S., and Wang, S. (2008). Periodontal ligament stem cell-mediated treatment for periodontitis in miniature swine. Stem Cell. *26*, 1065–1073. https://doi.org/10.1634/stemcells.2007-0734.
22. Wei, F., Song, T., Ding, G., Xu, J., Liu, Y., Liu, D., Fan, Z., Zhang, C., Shi, S., and Wang, S. (2013). Functional tooth restoration by allogeneic mesenchymal stem cell-based bio-root regeneration in swine. Stem Cells Dev. *22*, 1752–1762. https://doi.org/10.1089/scd.2012.0688.
23. Du, J., Shan, Z., Ma, P., Wang, S., and Fan, Z. (2014). Allogeneic bone marrow mesenchymal stem cell transplantation for periodontal regeneration. J. Dent. Res. *93*, 183–188. https://doi.org/10.1177/0022034513513026.
24. Hu, J., Cao, Y., Xie, Y., Wang, H., Fan, Z., Wang, J., Zhang, C., Wang, J., Wu, C.T., and Wang, S. (2016). Periodontal regeneration in swine after cell injection and cell sheet transplantation of human dental pulp stem cells following good manufacturing practice. Stem Cell Res. Ther. *7*, 130. https://doi.org/10.1186/s13287-016-0362-8.
25. Li, Z., Jiang, C.M., An, S., Cheng, Q., Huang, Y.F., Wang, Y.T., Gou, Y.C., Xiao, L., Yu, W.J., and Wang, J. (2014). Immunomodulatory properties of dental tissue-derived mesenchymal stem cells. Oral Dis. *20*, 25–34. https://doi.org/10.1111/odi.12086.
26. Kim, J., and Hematti, P. (2009). Mesenchymal stem cell-educated macrophages: a novel type of alternatively activated macrophages. Exp. Hematol. *37*, 1445–1453. https://doi.org/10.1016/j.exphem.2009.09.004.
27. Hao, S., Meng, J., Zhang, Y., Liu, J., Nie, X., Wu, F., Yang, Y., Wang, C., Gu, N., and Xu, H. (2017). Macrophage phenotypic mechanomodulation of enhancing bone regeneration by superparamagnetic scaffold upon magnetization. Biomaterials *140*, 16–25. https://doi.org/10.1016/j.biomaterials.2 017. 06.013.
28. Li, J., Jiang, X., Li, H., Gelinsky, M., and Gu, Z. (2021). Tailoring materials for modulation of macrophage fate. Adv. Mater. *33*, e2004172. https://doi.org/10.1002/adma.202004172.
29. Zhang, Q.Z., Nguyen, A.L., Yu, W.H., and Le, A.D. (2012). Human oral mucosa and gingiva: a unique reservoir for mesenchymal stem cells. J. Dent. Res. *91*, 1011–1018. https://doi.org/10.1177/00220345124610 6.
30. Li, Y., Kong, N., Li, Z., Tian, R., Liu, X., Liu, G., Wang, K., and Yang, P. (2019). Bone marrow macrophage M2 polarization and adipose-derived stem cells osteogenic differentiation synergistically promote rehabilitation of bone damage. J. Cell. Biochem. *120*, 19891–19901. https://doi.org/10.1002/jcb.29297.
31. Zhang, Q.Z., Su, W.R., Shi, S.H., Wilder-Smith, P., Xiang, A.P., Wong, A., Nguyen, A.L., Kwon, C.W., and Le, A.D. (2010). Human gingiva-derived mesenchymal stem cells elicit polarization of M2 macrophages and enhance cutaneous wound healing. Stem Cell. *28*, 1856–1868. https://doi.org/10.1002/stem.503.
32. Maggini, J., Mirkin, G., Bognanni, I., Holmberg, J., Piazzón, I.M., Nepomnaschy, I., Costa, H., Cañones, C., Raiden, S., Vermeulen, M., and Geffner, J.R. (2010). Mouse bone marrow-derived mesenchymal stromal cells turn activated macrophages into a regulatory-like profile. PLoS One *5*, e9252. https://doi.org/10.1371/journal.pone.0009252.
33. Cao, C., Tarlé, S., and Kaigler, D. (2020). Characterization of the immunomodulatory properties of alveolar bone-derived mesenchymal stem cells. Stem Cell Res. Ther. *11*, 102. https://doi.org/10.1186/s13287-020-01605-x.
34. Liu, J., Chen, B., Bao, J., Zhang, Y., Lei, L., and Yan, F. (2019). Macrophage polarization in periodontal ligament stem cells enhanced periodontal regeneration. Stem Cell Res. Ther. *10*, 320. https://doi.org/10.1186/s13287-019-1409-4.
35. Chen, X., Yang, B., Tian, J., Hong, H., Du, Y., Li, K., Li, X., Wang, N., Yu, X., and Wei, X. (2018). Dental follicle stem cells ameliorate lipopolysaccharide-induced inflammation by secreting TGF-beta 3 and TSP-1 to elicit macrophage M2 polarization. Cell. Physiol. Biochem. *51*, 2290–2308. https://doi.org/10.1159/000495873.
36. Shapouri-Moghaddam, A., Mohammadian, S., Vazini, H., Taghadosi, M., Esmaeili, S.A., Mardani, F., Seifi, B., Mohammadi, A., Afshari, J.T., and Sahebkar, A. (2018). Macrophage plasticity, polarization, and function in health and disease. J. Cell. Physiol. *233*, 6425–6440. https://doi.org/10.1002/jcp.26429.
37. Deshmane, S.L., Kremlev, S., Amini, S., and Sawaya, B.E. (2009). Monocyte chemoattractant protein-1 (MCP-1): an overview. J. Interferon Cytokine Res. *29*, 313–326. https://doi.org/10.1089/jir.2008.0027.
38. Griffith, J.W., Sokol, C.L., and Luster, A.D. (2014). Chemokines and chemokine receptors: positioning cells for host defense and immunity. Annu. Rev. Immunol. *32*, 659–702. https://doi.org/10.1146/annur ev-immunol-032713-120145.
39. Roca, H., Varsos, Z.S., Sud, S., Craig, M.J., Ying, C., and Pienta, K.J. (2009). CCL2 and interleukin-6 promote survival of human CD11b (+) peripheral blood mononuclear cells and induce M2-type macrophage polarization. J. Biol. Chem. *284*, 34342–34354. https://doi.org/10.1074/jbc.M109.042671.
40. Zhuang, Z., Yoshizawa-Smith, S., Glowacki, A., Maltos, K., Pacheco, C., Shehabeldin, M., Mulkeen, M., Myers, N., Chong, R., Verdelis, K., et al. (2019). Induction of M2 macrophages prevents bone loss in murine periodontitis models. J. Dent. Res. *98*, 200–208. https://doi.org/10.1177/0022034518805984.
41. Giri, J., Das, R., Nylen, E., Chinnadurai, R., and Galipeau, J. (2020). CCL2 and CXCL12 derived from mesenchymal stromal cells cooperatively polarize IL-10^{+} tissue macrophages to mitigate gut injury. Cell Rep. *30*, 1923–1934.e4. https://doi.org/10.1016/j.celrep.2020.01.047.
42. Do, D.C., Mu, J., Ke, X., Sachdeva, K., Qin, Z., Wan, M., Ishmael, F.T., and Gao, P. (2019). miR-511-3p protects against cockroach allergen-induced lung inflammation by antagonizing CCL2. Jci Insight *4*, e126832. https://doi.org/10.1172/jci.insight.126832.
43. Shen, Z., Kuang, S., Zhang, M., Huang, X., Chen, J., Guan, M., Qin, W., Xu, H.H.K., and Lin, Z. (2021). Inhibition of CCL2 by bindarit alleviates diabetes-associated periodontitis by suppressing inflammatory monocyte infiltration and altering macrophage properties. Cell. Mol. Immunol. *18*, 2224–2235. https://doi.org/10.1038/s41423-020-0500-1.

STAR★METHODS

KEY RESOURCES TABLE

REAGENT or RESOURCE	SOURCE	IDENTIFIER
Antibodies		
Rabbit anti-Arginase 1 (ARG1)	Abclonal	Cat# A4923; RRID: AB_2863390
Mouse anti-β-Actin	Applygen	Cat# C1313
Mouse anti-CD68	Abcam	Cat# ab955; RRID: AB_307338
Rabbit anti-CD163	Abclonal	Cat# A8383; RRID: AB_2768771
Rabbit anti-CD80	Abclonal	Cat# A16039; RRID: AB_2763477
Rabbit anti-Ki67	Abcam	Cat# ab15580; RRID: AB_443209
Rabbit anti-CD206	Cell Signaling Technology	Cat# 24595S
Goat anti-Mouse IgG (H+L) Highly Cross-Adsorbed Secondary Antibody, Alexa Fluor™ Plus 488	Thermo Fisher	Cat# A32723; RRID: AB_2633275
Goat anti-Rabbit IgG (H+L) Cross-Adsorbed Secondary Antibody, Alexa Fluor™ 594	Thermo Fisher	Cat# A-11012; RRID: AB_2534079
Chemicals, peptides, and recombinant proteins		
Minimum Essential Medium α	Gibco	Cat# 12571063
Fetal bovine serum	Gibco	Cat# 10099141C
L-glutamine	Gibco	Cat# 25030081
Penicillin-streptomycin	Gibco	Cat# 15070063
Vitamin C	Sigma-Aldrich	Cat# 1043003
RPMI 1640	Gibco	Cat# 11875119
Bovine serum albumin	Beyotime	Cat# ST023
Fluoroshield ™ with DAPI	Sigma-Aldrich	Cat# F6057
C-C motif chemokine ligand 2 (CCL2) neutralising antibody	R&D System	Cat# MAB679-500
Rcombinant human CCL2	Peprotech	Cat# 300-04
Lipopolysaccharides, LPS	MedChemExpress	Cat# HY-D1056
Recombinant Human IFN gamma	Novoprotein	Cat# C014
Phorbol-12-myristate-13-acetate, PMA	Sigma-Aldrich	Cat# 524400
Critical commercial assays		
ELISA MAX™ Deluxe Set Human TNF-α	Biolegend	Cat# 430204
ELISA MAX™ Deluxe Set Human IL-10	Biolegend	Cat# 430604
ELISA MAX™ Deluxe Set Human MCP-1/CCL2	Biolegend	Cat# 438804
BCA Protein Assay Kit	Solarbio	Cat# PC0020
RNAprep Pure Cell/Bacteria Kit	Tiangen Biotech	Cat# DP430
RNAprep pure Tissue Kit	Tiangen Biotech	Cat# DP431
FastKing RT Kit	Tiangen Biotech	Cat# KR116
SuperReal PreMix Plus	Tiangen Biotech	Cat# FP205
One Step TUNEL Apoptosis Assay Kit	Beyotime	Cat# C1090
Deposited data		
Raw microarray data from DPSCs and BMMSCs	This paper	GEO: GSE217636
Experimental models: Cell lines		
THP-1 cell line	Procell Life Science & Technology	CL-0233

(*Continued on next page*)

Continued

REAGENT or RESOURCE	SOURCE	IDENTIFIER
Experimental models: Organisms/strains		
Human bone marrow stem cells	Beijing Institute of Radiation Medicine	N/A
Human adipose-derived stem cells	Beijing Institute of Radiation Medicine	N/A
Human periodontal ligament stem cells	Beijing Institute of Radiation Medicine	N/A
Human dental pulp stem cells	Beijing Institute of Radiation Medicine	N/A
C57BL/6 mice	SPF (Beijing) Biotechnology	N/A
Software and algorithms		
SPSS 19.0	IBM	https://www.ibm.com/cn-zh/spss
Prism 8	GraphPad	https://www.graphpad.com/
Adobe Photoshop CC	Adobe	https://www.adobe.com/products/photoshop.html
Fiji	NIH Image	https://imagej.net/ij/download.html

RESOURCE AVAILABILITY

Lead contact

Further information and requests for resources and reagents should be directed to and will be fulfilled by the lead contact, Hu lei: hulei@ccmu.edu.en.

Materials availability

All materials are available upon request.

Data and code availability

Data: The expression data have been deposited in Gene Expression Omnibus (GEO) under the primary accession code GSE217636.
Code: This paper does not report original code.
Other items: No other new unique reagent was generated. Any additional information required to reanalyze the data reported in this paper is available from the lead contact upon request.

EXPERIMENTAL MODEL AND STUDY PARTICIPANT DETAILS

Mice

All animal use was approved by the Animal Care Committee of the Beijing Stomatology Hospital, Capital Medical University. Mice were maintained on a 12 h light/dark cycle, and food and water was provided *ad libitum*. All mice were healthy with no obvious behavioural phenotypes. Male C57BL/6J mice (8 weeks old) were obtained from SPF (Beijing) Biotechnology.

METHOD DETAILS

Mesenchymal cells cultures

Human BMMSCs, ADSCs, PDLSCs and DPSCs were isolated from iliac bone marrow, adipose tissue, dental pulp and periodontal tissue and obtained from the Department of Experimental Haematology, Beijing Institute of Radiation Medicine. The same passage of BMMSCs, ADSCs, PDLSCs and DPSCs were used for each experiment. Cells were cultured in Minimum Essential Medium α (α-MEM; Gibco, Grand Island, NY, USA) containing 10% fetal bovine serum (FBS, Gibco), 1% L-glutamine (Gibco), 1% penicillin-streptomycin (Gibco) under standard culture conditions (37°C, 95% humidified air and 5% CO_2). The medium was changed every 2-3 days.

Transplantation in C57BL/6 mice

MSCs sheets were generated as described by Wei et al. [13]. 1.5×10^5 PDLSCs, DPSCs, ADSCs and BMMSCs at passage four were subcultured in 60 mm dishes. 20 μg/mL Vc (Sigma-Aldrich Corp., St. Louis, MO, USA) was added to the culture medium. After 10-14 days, the cells at the edge of the dishes wrapped, which means that cell sheets had formed and could be detached. A complete Vc-induced DPSCs, PDLSCs, BMMSCs and ADSCs sheets were mixed with 40 mg of sterile HA/TCP ceramic particles and transplanted subcutaneously into the dorsal surface of C57BL/6 mice (n=5). At 8 weeks after transplantation, all animals were sacrificed, and the samples were harvested. Part of samples were grinded and then total RNA collected by RNAprep pure Tissue Kit (DP431, Tiangen Biotech, Beijing, China). The others fixed with 4% paraformaldehyde, decalcified with buffered 10% EDTA (pH 8.0), and then embedded in paraffin. 5 μm sections were obtained, deparaffinized, hydrated and stained with hematoxylin and eosin (HE) staining, immunohistochemistry and immunofluorescence.

THP-1 cells culture and stimulation

THP-1, a human monocyte cell line, was cultured in complete RPMI 1640 (Gibco) containing 10% FBS (Gibco), 1% penicillin, streptomycin and L-glutamine (Thermo Fisher, Waltham, USA) at 37°C with 5% CO_2. Culture medium was changed every 2-3 days as necessary. For differentiation to naive macrophages, THP-1 were incubated with 100 ng/mL phorbol 12-myristate 13-acetate (PMA, Sigma-Aldrich) in 6-well plates for 24 h. Following differentiation, the plates were replaced by fresh medium, and cells were cultured for another 24 h for THP-1 M0 macrophage. For M1 polarization, M0 in fresh medium were co-stimulated with LPS (1 μg/mL, HY-D1056, MedChemExpress, New Jersey, USA) and IFNγ (50 ng/mL, C014, Novoprotein, Shanghai, China), and M0 were incubated with the corresponding stimuli for 24 h without media replacement.

Preparation of conditioned medium (CM)

Human DPSCs and BMMSCs, 70-80% confluent, were rinsed with phosphate-buffered saline (PBS), and fed serum-free α-MEM (Gibco) containing 1% L-glutamine, penicillin and streptomycin. The medium was collected after 24 h, centrifuged for 5 minutes at 1500 rpm and then for another 3 minutes at 3000 rpm to remove cells, filtered at 0.22 μm (Millex™ GP Filter Unit; Merck Millipore Ltd, Darmstadt, Germany), and stored at -20°C within 2 weeks or at -80°C within 1 month until use.

THP-1 cells cultured with CM

THP-1 macrophages (6×10^5) were seeded in 6-well plates. THP-1 M0 macrophage and M1 macrophage cells were cultured with fresh complete medium (complete RPMI 1640 medium: complete α-MEM medium = 3: 2) for 3 d. In DPSCs-CM group, cells were cultured by mixture of 2/5 complete RPMI 1640 medium, 27/50 DPSCs-CM and 3/50 FBS. In BMMSCs-CM group, cells were cultured by mixture of 2/5 complete RPMI 1640 medium, 27/50 BMMSCs-CM and 3/50 FBS for 3 d.

THP-1 cells co-cultured with BMMSCs and DPSCs by transwell assay

THP-1 macrophages (6×10^5) were seeded in the lower chamber of the transwell, while DPSCs or BMMSCs (3×10^5) were loaded into the upper chamber of transwell insert (Corning, New York, NY, USA) with each type of cell cultured alone as control. Under certain conditions, THP-1 macrophages and DPSCs or BMMSCs (2: 1) of passage 4 and DPSCs of passage 8 were cocultured in a transwell system in the presence or absence of either 10 μg/mL C-C motif chemokine ligand 2 (CCL2) neutralising antibody (MAB679; R&D System, Minnesota, USA) for 3 d. And recombinant human CCL2 (10 ng/mL or 15 ng/mL; 300-04; Peprotech, Rocky Hill, USA) were added for 3 d as positive control group. Then the culture media and whole cell lysates of THP-1 macrophages were prepared for quantitative real-time polymerase chain reaction (qRT-PCR), immunofluorescent staining, western blotting, and enzyme-linked immunosorbent assay (ELISA), respectively.

Bioinformatic analysis gene expression profile of BMMSCs and DPSCs

Bioinformatic analysis gene expression profile of BMMSCs and DPSCs gene expression datasets derived from GEO Series accession number GSE217636 (https://www.ncbi.nlm.nih.gov/geo/query/acc.cgi?acc=GSE217636), in which gene expression between human BMMSCs and DPSCs was compared. Those genes with an adjusted $P < 0.05$ and absolute value of fold change (FC) > 2 were analysed. Then differentially expressed genes related to immune were selected and verified by qRT-PCR.

qRT-PCR

Total RNA was extracted from macrophages with RNAprep Pure Cell/Bacteria Kit (DP430; Tiangen Biotech, Beijing, China) and were reversely transcribed to cDNA with FastKing RT Kit (KR116; Tiangen Biotech, Beijing, China) according to the manufacturer's instructions. qRT-PCR was performed using an SuperReal PreMix Plus (SYBR Green) (FP205; Tiangen Biotech, Beijing, China). The PCR mixture comprised of 10 μL SYBR, 0.6 μM forward and reverse primers and 1 μL cDNA. After normalization of target gene expression, the data was quantified by the $2^{-\Delta\Delta Ct}$ method. The genes and primer sequences are listed in Table S1.

Western blot

Cell extracts were prepared with whole cell lysis buffer (C1053, Applygen, Beijing, China) according to the manufacturer's instructions. The protein concentrations were determined by the BCA Protein Assay Kit (PC0020; Solarbio, Beijing, China). Equal amounts of cellular proteins (20 μg) were boiled for 10 min at 98°C. Equal amounts of protein extracts were loaded onto 10% polyacrylamide gels for electrophoresis and transferred to nitrocellulose membranes. Bands were detected immunologically with polyclonal antibodies (1: 1000) against Arginase 1 (A4923; Abclonal, Wuhan, Hubei, China). β-Actin (C1313; Applygen) was used as a loading control. Immunoblot bands were visualized following the application of ECL detection system (ChemiDoc™ MP Imaging System, Biorad, California, USA).

Enzyme-linked immunosorbent assay (ELISA)

Cell free supernatants were collected and centrifuged at 14000 rpm for 30 min at 4°C of each group and assayed for the concentration of TNF-α, IL-10 and CCL2 with ELISA kits (human TNF-α, 430204; human IL-10, 430604; human CCL2, 438804; Biolegend, California, USA)

following the manufacturer's instructions. The optical density was measured at 450 nm using a microplate reader with the correction wavelength set at 570 nm.

Wound healing model and BMMSCs and DPSCs treatment

Male C57BL6 mice (n=5, body weights of 20-22 g) were anesthetized with pentobarbital sodium (50 mg/kg). For the wound healing model of palatal mucosa, the full-thickness palate ranging from the mesial edge of the first molar to the distal edge of the third molar, from gingival margin to palatal suture was removed. For treatment, mice were randomized to different treatment groups. Unless otherwise stated, 2.5×10^5 engineered DPSCs and BMMSCs at passage 5 suspended in PBS and recombinant human CCL2 (10 μg/mice) were directly injected into the surrounding mucosa in day 1. Neutralising antibodies to human CCL2 (R&D Systems, Minnesota, USA) were given to mice by intraperitoneal injection in day 2 at a dose of 10 μg/mouse. The mice were sacrificed after 5 days, and the defect area in palates was observed by stereomicroscopy and assessed using ImageJ (NIH, MD, United States).

Immunofluorescence staining

THP-1 cells were adhered to the surface of glass cover slides were transferred to transwell systems or conditioned medium. After coculture, cells on the slides were fixed with 4% paraformaldehyde for 30 min, permeabilized with 0.3% Triton (MP Biomedicals, California, USA) for 10 min and then blocked with 3% bovine serum albumin (BSA; Beyotime) for 30 min at room temperature. Slides were incubated separately with antibodies against CD68 (1/100, ab955; Abcam, Massachusetts, US), CD163 (1/100, A8383; Abclonal) and CD80 (1/100, A16039; Abclonal) at 4°C overnight. The sections (5 μm) of paraffin-embedded tissue were stained with specific antibodies (1: 100) for Ki67 (ab15580, Abcam,), CD68 (ab955, Abcam,), CD206(24595S, Cell Signaling Technology, CST, Boston, USA) and ARG1(A4923, Abclonal) overnight at 4°C and subsequently incubated with secondary antibodies (1: 1000, A32723, A-11012, Thermo fisher) plus Fluoroshield TM with DAPI (Sigma-Aldrich). Double-stained samples were evaluated under a fluorescence microscope (BX61, Olympus, Tokyo, Japan).

Terminal deoxynucleotidyl transferase dUTP nick end labeling (TUNEL) assay

Paraffinized samples were sectioned at 5 μm thickness, mounted on silane-coated glass slides. TUNEL staining was performed with a One Step TUNEL Apoptosis Assay Kit (C1090; Beyotime, Shanghai, China) according to the manufacturer's instructions. Images were captured under a confocal microscope and the number of TUNEL-positive cells was calculated using Image J software (NIH, MD, United States).

QUANTIFICATION AND STATISTICAL ANALYSIS

The results are presented as mean ± SDs. Student's t-test was employed to compare difference between two groups with normal distribution. The one-way ANOVA test was used to determine significant differences among multiple groups, and the Bonferroni method was used to compare the inter-group variation. The Kruskal-Wallis test was employed to compare difference with non-normal distribution. And $P < 0.05$ was considered statistically significant (* $P < 0.05$, ** $P < 0.01$). Statistical analysis was performed using SPSS 19.0. Statistical analysis was conducted using GraphPad Prism 8 software (San Diego, CA, USA). Number of experiments and statistical information are stated in the corresponding figure legends. In figures, asterisks denote statistical significance marked by ^{ns}, $P > 0.05$; *, $P < 0.05$; **, $P < 0.01$; ***, $P < 0.001$.